A Rod-Packing Microporous Hydrogen-Bonded Organic Framework for Highly Selective Separation of C_2H_2/CO_2 at Room Temperature**

*Peng Li, Yabing He, Yunfeng Zhao, Linhong Weng, Hailong Wang, Rajamani Krishna, Hui Wu, Wei Zhou, Michael O'Keeffe, Yu Han, and Banglin Chen**

Abstract: Self-assembly of a trigonal building subunit with diaminotriazines (DAT) functional groups leads to a unique rod-packing 3D microporous hydrogen-bonded organic framework (HOF-3). This material shows permanent porosity and demonstrates highly selective separation of C_2H_2/CO_2 at ambient temperature and pressure.

Development of new porous adsorbents is a very important topic for adsorption-based gas separations. For example, extensive research on porous metal–organic frameworks (MOFs) has not only led to a number of new MOF adsorbents whose separation selectivities and capacities have surpassed those traditional zeolite materials for some important CO_2/N_2, CO_2/CH_4, CO_2/H_2, and xylene isomer separations,[1,2] but also generated a few MOFs to target the very challenging C_2H_2/C_2H_4,[3] C_2H_4/C_2H_6, C_3H_6 and C_3H_8,[4,5] and CO/N_2 separations.[6]

Among diverse gas separations, C_2H_2/CO_2 is another very challenging mixture. This is because these two gas molecules have very similar shapes, dimensions ($332 \times 334 \times 570$ pm versus $318.9 \times 333.9 \times 536.1$ pm), and boiling points ($-84\,°C$ versus $-78.5\,°C$).[7] Since the discovery of the first MOF material for this separation,[8] several MOFs have been realized for this important gas separation, though the selectivities are quite low.[9]

Recently we, and several other groups, have realized that it is feasible to make use of hydrogen bonding interactions to construct new porous materials which we have termed as hydrogen bonded organic frameworks (HOFs),[10] providing the new approach to develop and explore new porous adsorbents for gas separations. In fact, the first, HOF-1, exhibits superior C_2H_2/C_2H_4 separation to other MOFs.[10h] Compared with MOFs, HOFs have some advantages including solution processability and characterization, easy purifi-

cation, and straightforward regeneration and reusage by simple recrystallization. Because the pore surfaces within HOFs are apparently different from those within MOFs and zeolites, exploration of HOF materials might lead to some unique new adsorbents for gas separations.

Herein we report a new system, HOF-3, constructed from a new triangular organic linker containing three hydrogen-bonding motifs of 2,4-diaminotriazinyl (DAT) (Figure 1a). Unlike those reported HOFs whose porous structures were built from discrete building units; HOF-3, to the best of our knowledge, is the first example of HOFs constructed from one-dimensional rod-packing units exhibiting the **srs** topology. More importantly, the activated HOF-3a shows superior selectivity for C_2H_2/CO_2 separation to the established MOF materials.

The triangular organic building block 3-DAT, shown in Figure 1a, can be readily synthesized in 84% yield by the reaction of the corresponding nitrile with dicyandiamide (Supporting Information, Scheme S1). The colorless block crystals of HOF-3 suitable for X-ray diffraction analysis were grown by slow vapor diffusion of THF into a large vial containing saturated DMSO solution of this building block for a week under room temperature. The purity of HOF-3 was confirmed by ^1H NMR and ^{13}C NMR spectroscopy, thermogravimetric analysis (TGA), and powder X-ray diffraction (PXRD; Supporting Information, Figures S1–S3). The inclusion of the solvent molecules into the framework leads to the HOF-3 whose phase is different from that of the as-synthesized 3-DAT. TGA curve indicates that the framework of HOF-3 can be stable up to 350 °C.

Single-crystal X-ray diffraction reveals that HOF-3 crystallized in the rhombohedral space group $R3$ and HOF-3 is a three-dimensional rod-packing porous material with one-dimensional hexagonal channels of about 7.0 Å in diameter

---

[*] P. Li,[+] Dr. Y. He,[+] Dr. H. Wang, Prof. Dr. B. Chen
Department of Chemistry, University of Texas at San Antonio
One UTSA Circle, San Antonio, TX 78249-0698 (USA)
E-mail: banglin.chen@utsa.edu
Homepage: http://www.utsa.edu/chem/chen.html

Prof. Dr. L. Weng
Department of Chemistry, Fudan University
220 Handan Rd, Shanghai 200433 (China)

Prof. Dr. R. Krishna
Van't Hoff Institute for Molecular Sciences
University of Amsterdam
Science Park 904, 1098 XH Amsterdam (The Netherlands)

Prof. Dr. M. O'Keeffe
Department of Chemistry and Biochemistry
Arizona State University (USA)

Prof. Dr. H. Wu, Prof. Dr. W. Zhou
NIST Center for Neutron Research
Gaithersburg, MD 20899-6102 (USA)
and
Department of Materials Science and Engineering
University of Maryland, College Park, MD 20742 (USA)

Dr. Y. Zhao, Prof. Dr. Y. Han
Advanced Membranes and Porous Materials Center
Physical Sciences and Engineering Division
King Abdullah University of Science and Technology
Thuwal 23955-6900 (Saudi Arabia)

[+] These authors contributed equally to this work.
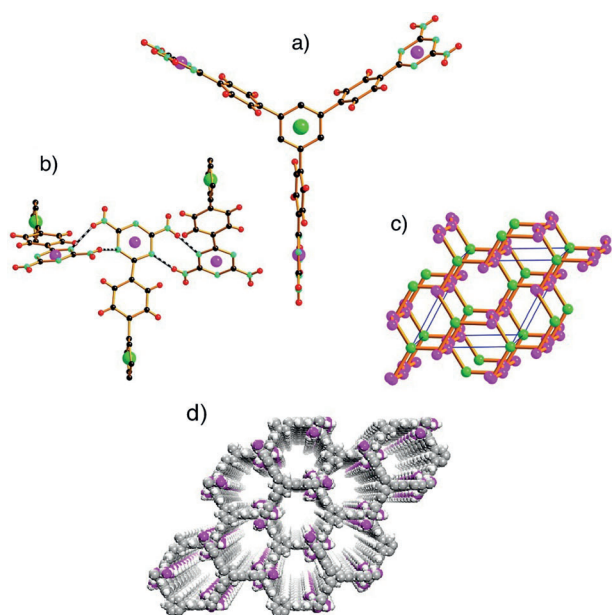

Figure 1. X-ray crystal structure of HOF-3 featuring a) the basic organic building block in which the centers of central benzene ring (green balls) and centers of three 1,3,5-triazine rings (magenta balls) act as nodes; b) The H-bonded link between DAT groups showing that each is joined to two other DAT groups; c) The net of 3-c branch points as it occurs in the crystal structure; and d) three-dimensional packing showing the 1D hexagonal channels of about 7.0 Å in diameter along the *c* axis (C gray, H white, N pink).

(Figure 1 d). The tritopic building unit has a 3-coordinated (3-c) node (A) at its center shown as a green ball in Figure 1 a. The three DAT groups shown as magenta balls (B) in the Figure 1 a are linked to two other DAT groups by H-bonds as shown in Figure 1 b, so each of these also corresponds to a 3-c node. The connectivity is A-B$_3$ and B-AB$_2$. The 3-c net is the ubiquitous **srs** (Figure 1 c), which can be described (see the Supporting Information) as parallel threefold helical rods (B) linked by additional 3-c nodes (A) into a 3-D net (Supporting Information, Figure S4). Initially, we tried to use the discrete molecule approach to rationalize the topology. However, the rationalized structure of NaCl topology apparently does not make much sense and is far away from the pore nature. It was then termed as a rod-packing topology to suitably describe the framework channels.[11] The pore spaces within the frameworks encapsulate certain amount of disordered DMSO and THF solvent molecules.

The available void space and high thermal stability of HOF-3 prompts us to examine the gas adsorption properties of HOF-3. The as-synthesized HOF-3 was exchanged with acetone several times then evacuated under dynamic vacuum to obtain desolvated HOF-3 a, which does not take up any N$_2$ gas molecules at 77 K. Such phenomena have been commonly observed in HOF and supramolecular organic framework (SOF) materials,[10f–h] though the exact reasons are still not clear. However, the CO$_2$ gas sorption isotherm of HOF-3 a at 196 K clearly indicates its microporous nature with Brunauer–Emmett–Teller (BET) surface area of 165.0 m^{2}g^{-1} (Supporting Information, Figure S5), which is moderate.[10] Interestingly, HOF-3 a takes up quite different amounts of C$_2$H$_2$

and CO$_2$ at room temperature. The C$_2$H$_2$ uptakes of 58 cm^{3}g^{-1} at 273 K and 47 cm^{3}g^{-1} at 296 K are systematically about twice higher than CO$_2$ uptakes of 31 cm^{3}g^{-1} at 273 K and 21 cm^{3}g^{-1} at 296 K at 1 atm (Figure 2 a; Supporting Information, Figure S6). This is unusual given the fact that these two gas molecules are comparable in terms of their dimensions and boiling points.[9]

This discovery motivated us to examine its feasibility for the industrially important C$_2$H$_2$/CO$_2$ separation in more details. The pure component isotherm data were fitted with the dual-Langmuir isotherm model (Supporting Information, Figure S7). To understand the binding energy at low coverage, isosteric heats of adsorption of C$_2$H$_2$ and CO$_2$ in HOF-3 a are calculated. Data on the loading dependence of Q_{st} in HOF-3 a are presented in the Supporting Information, Figure S8. Particularly remarkable is the relatively low value (< 20 kJ mol^{-1}) of the isosteric heat of adsorption for C$_2$H$_2$. To underscore this point, Figure 2 b presents a comparison of the heats of adsorption of C$_2$H$_2$ in various MOFs (UTSA-30a,[9a] UTSA-50a,[9b] and CuBTC).[5] We note that value of Q_{st} in HOF-3 a is significantly lower than that for MOFs. The value of Q_{st} in HOF-3 a is systematically more than twice lower than that in CuBTC with coordinately unsaturated metal sites (Figure 2 b). These data highlight that HOF-3 a is a promising material for the separation of C$_2$H$_2$/CO$_2$ with lower regeneration energy requirement for C$_2$H$_2$.

We further performed calculation using the Ideal Adsorbed Solution Theory (IAST) of Myers and Prausnitz.[12] Figure S9 presents IAST calculations of the component loadings for C$_2$H$_2$ and CO$_2$ in binary equimolar mixture as a function of the total bulk gas-phase pressure at 296 K, and Figure 2 c provides a comparison of the adsorption selectivity of C$_2$H$_2$/CO$_2$ in equimolar mixtures in HOF-3 a and the three other MOFs at 296 K. We note that adsorption selectivity of HOF-3 a is significantly higher than that of other MOFs. Though at zero-coverage the selectivity of UTSA-50a (15) is higher than that of HOF-3 a (14), as the pressure increases to 100 kPa, the adsorption selectivity increases to 21 for HOF-3 a, while for MOF materials, the selectivity reduces significantly (lower than 6).

Preliminary studies on the breakthrough simulations for C$_2$H$_2$/CO$_2$ mixtures using the established methodology described in early publications of Krishna (Supporting Information, Figure S10) indicate that it is feasible for HOF-3 a to separate C$_2$H$_2$ from the C$_2$H$_2$/CO$_2$ mixture at room temperature (Supporting Information, Figure S11).[12b–d] That encouraged us to evaluate the actual performance of HOF-3 a through the experimental column breakthrough in which an equimolar C$_2$H$_2$/CO$_2$ mixture was flowed over a packed column of the HOF-3 a solid with a total flow of 5 cm^{3}min^{-1} at 296 K. As shown in Figure 2 d, the separation of C$_2$H$_2$/CO$_2$ mixture gases through a column packed with HOF-3 a solid can be efficiently achieved. To the best of our knowledge, this is the first example of porous materials whose separation for C$_2$H$_2$/CO$_2$ mixture has been clearly established by experimental breakthrough, enabling HOF-3 a to be a potential material for industrial acetylene purification application.

To help understand the C$_2$H$_2$/CO$_2$ selectivity in HOF-3 a, we performed detailed computational investigations. We first
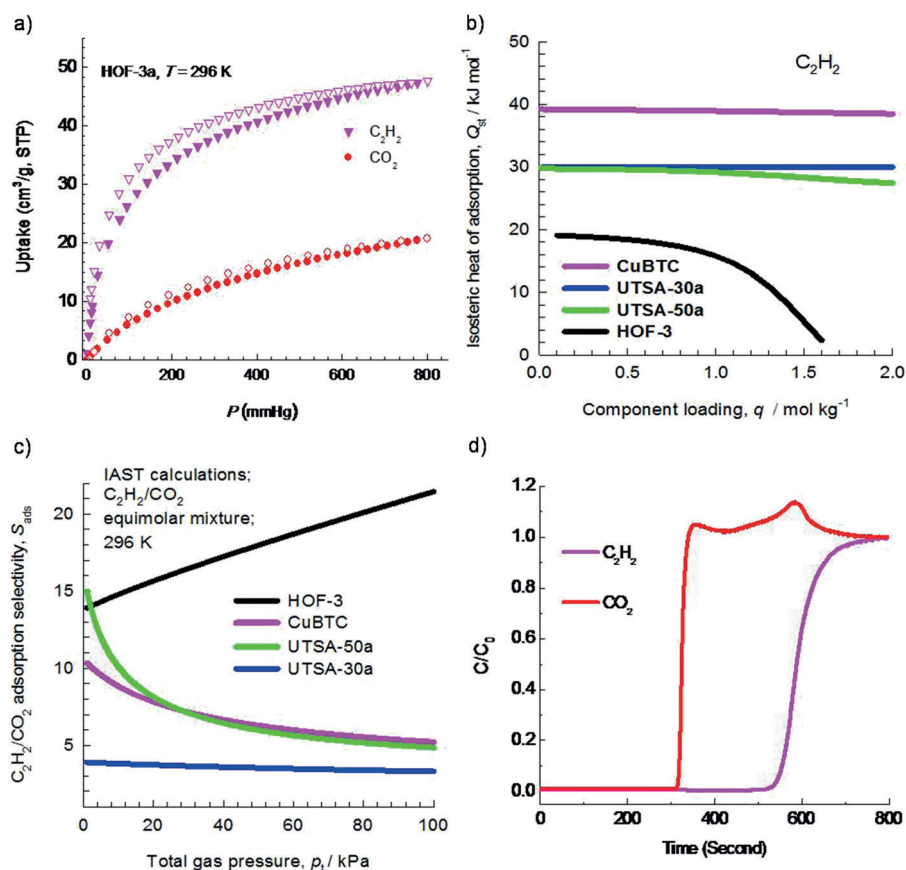
Figure 2. a) Sorption isotherms of C_2H_2 and CO_2 of HOF-3 a at 296 K; b) comparison of the heats of adsorption of C_2H_2 in HOF-3 a and various MOFs; c) IAST adsorption selectivities of C_2H_2/CO_2 in equimolar mixture in HOF-3 a and various MOFs at 296 K; and d) experimental column break-through curve for an equimolar C_2H_2/CO_2 mixture (296 K, 1 bar) in an adsorber bed packed with HOF-3 a.

much more "localized" than C_2H_2 in terms of position and orientation, with the adsorption energy decaying rapidly if the CO_2 molecule is moved away from the optimized position. For C_2H_2, the adsorption potential surface is much "flatter" in the region adjacent to the pocket site, and more than one molecule can be accommodated on each site simultaneously with similar binding strength. This subtle difference in the gas/HOF framework interaction is likely the reason why the uptake (that is, surface coverage) of C_2H_2 is higher than CO_2 in HOF-3 a at RT.

In summary, we have targeted a three-dimensional rod-packing HOF for highly selective C_2H_2/CO_2 separation at ambient temperature and pressure. To the best of our knowledge, this is the first example of rod-packing porous hydrogen-bonded organic frameworks. More importantly, its C_2H_2/CO_2 separation selectivities are systematically higher than those found in the well-established MOF materials, highlighting the bright promise of such new porous HOF materials for gas separation. Such preferential adsorption of HOF-3 for acetylene over carbon dioxide is attributed to the unique pockets and pore surfaces within HOF-3. It is expected that extensive research endeavors on porous HOFs will facilitate the discoveries of new porous HOFs for gas separation and other important applications in the near future.

optimized the HOF-3 a structure by first-principles DFT-D (dispersion-corrected density-functional theory) calculations,[13] and then carried out grand canonical Monte Carlo (GCMC) simulations using the classical force field method (for details, see the Supporting Information). The simulated PXRD of the optimized HOF-3 a structure matches with the experimental structure of HOF-3 a quite well (Supporting Information, Figure S3), indicating that the results from simulation studies are quite reasonable. HOF-3 a is the slightly shrunk form of HOF-3, keeping identical framework connectivity. From the probability distribution of adsorbed gas molecules generated from the simulations (Supporting Information, Figure S12), we found that for both C_2H_2 and CO_2, the adsorption takes place mainly adjacent to the "pocket" between two H-bonded DAT groups. We then introduced gas molecules at these sites, and further optimized the "HOF-3 a + gas" structures using DFT-D. We found that the gas binding is relatively weak in both cases, and of van der Waals type in nature. The derived static gas binding energies are 20.9 kJ mol^{-1} and 26.3 kJ mol^{-1} for C_2H_2 and CO_2, respectively, in qualitative agreement with the experimental Q_{st} values. Interestingly, we noticed that the relaxed, adsorbed CO_2 molecules (Supporting Information, Figure S13) are

Experimental Section

1632, 1578, 1533, 1449, 1433, 1396, 1255, 1227, 1016, 985, 907, 850, 808, 693, 666 cm⁻¹.

[1] a) J.-R. Li, J. Sculley, H.-C. Zhou, *Chem. Rev.* **2012**, *112*, 869; b) Z. J. Zhang, Y. G. Zhao, Q. H. Gong, Z. Li, J. Li, *Chem. Commun.* **2013**, *49*, 653; c) C. Wang, D. M. Liu, W. B. Lin, *J. Am. Chem. Soc.* **2013**, *135*, 13222.

[2] B. Chen, S. Xiang, G. Qiang, *Acc. Chem. Res.* **2010**, *43*, 1115.

[3] S. Xiang, Z. Zhang, C.-G. Zhao, K. Hong, X. Zhao, D.-R. Ding, M.-H. Xie, C.-D. Wu, M. C. Das, R. Gill, K. M. Thomas, B. Chen, *Nat. Commun.* **2011**, *2*, 204.

[4] a) E. D. Bloch, W. L. Queen, R. Krishna, J. M. Zadrozny, C. M. Brown, J. R. Long, *Science* **2012**, *335*, 1606; b) H. Furukawa, K. E. Cordova, M. O'Keeffe, O. M. Yaghi, *Science* **2013**, *341*, 974; c) C. Y. Lee, Y. S. Bae, N. C. Jeong, O. K. Farha, A. A. Sarjeant, C. L. Stern, P. Nickias, R. Q. Snurr, J. T. Hupp, S. T. Nguyen, *J. Am. Chem. Soc.* **2011**, *133*, 5228; d) P. Nugent, Y. Belmabkhout, S. D. Burd, A. J. Cairns, R. Luebke, K. Forrest, T. Pham, S. Q. Ma, B. Space, L. Wojtas, M. Eddaoudi, M. J. Zaworotko, *Nature* **2013**, *495*, 80; e) S. M. Chen, J. Zhang, T. Wu, P. Y. Feng, X. H. Bu, *J. Am. Chem. Soc.* **2009**, *131*, 16027; f) J. P. Zhang, X. M. Chen, *J. Am. Chem. Soc.* **2009**, *131*, 5516; g) J. P. Zhang, S. Kitagawa, *J. Am. Chem. Soc.* **2008**, *130*, 907; h) H. L. Jiang, Q. Xu, *Chem. Commun.* **2011**, *47*, 3351.

[5] Y. He, R. Krishna, B. Chen, *Energy Environ. Sci.* **2012**, *5*, 9107.

[6] H. Sato, W. Kosaka, R. Matsuda, A. Hori, Y. Hijikata, R. V. Belosludov, S. Sakaki, M. Takata, S. Kitagawa, *Science* **2014**, *343*, 167.

[7] Z. Zhang, S. Xiang, B. Chen, *CrystEngComm* **2011**, *13*, 5983.

[8] R. Matsuda, R. Kitaura, S. Kitagawa, Y. Kubota, R. V. Belosludov, T. C. Kobayashi, H. Sakamoto, T. Chiba, M. Takata, Y. Kawazoe, Y. Mita, *Nature* **2005**, *436*, 238.

[9] a) Y. He, S. Xiang, Z. Zhang, S. Xiong, F. R. Fronczek, R. Krishna, M. O'Keeffe, B. Chen, *Chem. Commun.* **2012**, *48*, 10856; b) H. Xu, Y. He, Z. Zhang, S. Xiang, J. Cai, Y. Cui, Y. Yang, G. Qian, B. Chen, *J. Mater. Chem. A* **2013**, *1*, 77.

[10] a) K. E. Maly, E. Gagnon, T. Maris, J. D. Wuest, *J. Am. Chem. Soc.* **2007**, *129*, 4306; b) J. H. Fournier, T. Maris, J. D. Wuest, *J. Org. Chem.* **2004**, *69*, 1762; c) J. D. Wuest, *Chem. Commun.* **2005**, 5830; d) P. S. Nugent, V. L. Rhodus, T. Pham, K. Forrest, L. Wojtas, B. Space, M. J. Zaworotko, *J. Am. Chem. Soc.* **2013**, *135*, 10950; e) X.-Z. Luo, X.-J. Jia, J.-H. Deng, J.-L. Zhong, H.-J. Liu, K.-J. Wang, D.-C. Zhong, *J. Am. Chem. Soc.* **2013**, *135*, 11684; f) J. Lü, C. Perez-Krap, M. Suyetin, N. H. Alsmail, Y. Yan, S. Yang, W. Lewis, E. Bichoutskaia, C. C. Tang, A. J. Blake, R. Cao, M. Schröder, *J. Am. Chem. Soc.* **2014**, *136*, 12828; g) P. Li, Y. He, J. Guang, L. Weng, J. C.-G. Zhao, S. Xiang, B. Chen, *J. Am. Chem. Soc.* **2014**, *136*, 547; h) Y. He, S. Xiang, B. Chen, *J. Am. Chem. Soc.* **2011**, *133*, 14570; i) M. Mastalerz, I. M. Oppel, *Angew. Chem. Int. Ed.* **2012**, *51*, 5252; *Angew. Chem.* **2012**, *124*, 5345.

[11] a) S. T. Hyde, M. O'Keeffe, D. M. Proserpio, *Angew. Chem. Int. Ed.* **2008**, *47*, 7996; *Angew. Chem.* **2008**, *120*, 8116; b) V. A. Blatov, M. O'Keeffe, D. M. Proserpio, *CrystEngComm* **2010**, *12*, 44.

[12] a) A. L. Myers, J. M. Prausnitz, *AIChE J.* **1965**, *11*, 121; b) R. Krishna, J. R. Long, *J. Phys. Chem. C* **2011**, *115*, 12941; c) R. Krishna, *Microporous Mesoporous Mater.* **2014**, *185*, 30; d) R. Krishna, R. Baur, *Sep. Purif. Technol.* **2003**, *33*, 213.

[13] P. Giannozzi, S. Baroni, N. Bonini, M. Calandra, R. Car, C. Cavazzoni, D. Ceresoli, G. L. Chiarotti, M. Cococcioni, I. Dabo, A. Dal Corso, S. Fabris, G. Fratesi, S. de Gironcoli, R. Gebauer, U. Gerstmann, C. Gougoussis, A. Kokalj, M. Lazzeri, L. Martin-Samos, N. Marzari, F. Mauri, R. Mazzarello, S. Paolini, A. Pasquarello, L. Paulatto, C. Sbraccia, S. Scandolo, G. Sclauzero, A. P. Seitsonen, A. Smogunov, P. Umari, R. M. Wentzcovitch, *J. Phys. Condens. Matter* **2009**, *21*, 395502.

A Rod-Packing Microporous Hydrogen-Bonded Organic Framework for Highly Selective Separation of C₂H₂/CO₂ at Room Temperature**

Peng Li, Yabing He, Yunfeng Zhao, Linhong Weng, Hailong Wang, Rajamani Krishna, Hui Wu, Wei Zhou, Michael O'Keeffe, Yu Han, and Banglin Chen*

anie_201410077_sm_miscellaneous_information.pdf

1. General remarks

All reagents and solvents were used as received from commercial suppliers without further purification. ^{1}H NMR and ^{13}C NMR spectrawere recorded on a Varian Mercury 300 MHz spectrometer. Tetramethylsilane (TMS) and deuterated solvents (CDCl$_3$, δ=77.00 ppm; DMSO-d_6, δ = 39.50 ppm)were used as internal standards in ^{1}H NMR and ^{13}C NMRexperiments, respectively.The coupling constants were reported in Hertz. FTIR spectra were performed on a Bruker Vector 22 spectrometer at room temperature.The elemental analyses were performed with Perkin–Elmer 240 CHN analyzers from Galbraith Laboratories, Knoxville.Thermogravimetric analyses (TGA) were measured using a Shimadzu TGA-50 analyzer under a nitrogen atmosphere with a heating rate of 5 $^{\circ}$Cmin^{-1}. Powder X–ray diffraction (PXRD) patternswere recorded by a Rigaku Ultima IV diffractometer operated at 40 kV and 44 mA with a scan rateof 1.0 degmin^{-1}. The crystallographic measurement wasperformed on an Bruker Apex II CCD diffractometer graphite-monochromatic enhanced ultra Curadiation (λ = 1.54178 Å) at 193 K. The structure was solved by direct methods and refined by fullmatrixleast-squares methods with the SHELX-97 program package.The solvent molecules in as-synthesized HOF crystal in are highly disordered.TheSQUEEZE subroutine of the PLATON software suit was used toremove the scattering from the highly disordered guest molecules. The resulting new files were used to further refine the structures. TheH atoms on C atoms were generated geometrically. A Micromeritics ASAP 2020 surface area analyzer was used to measure gas adsorption isotherms. To have a guest–free framework, the fresh sample was guest–exchanged with dry acetone at least 10 times, filtered and vacuumed at room temperature for 24 h and then at 373 K until the outgas rate was 5 μmHgmin^{-1} prior to measurements. A sample of 99.6 mg was used for the sorption measurements and was maintained at 196 K with a dry ice-acetone bath, at 273 K with an ice–water bath. As the center–controlled air conditioner was set up at 23 $^{\circ}$C, a water bath was used for adsorption isotherms at 296 K.

2. Synthesis and characterization of the organic linker
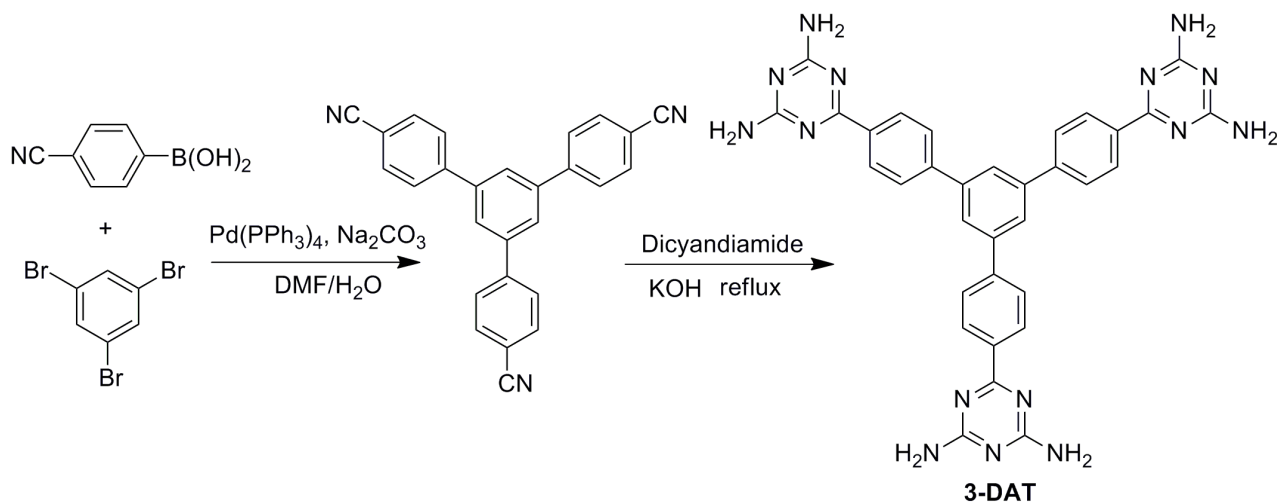
Scheme S1 The synthetic route to the organic building block.

1,3,5-tri(4-cyanophenyl)benzene: 4-cyanophenylboronic acid (4.20 g, 28.58 mmol, Frontier Scientific), 1,3,5-tribromobenzene (2.00 g, 6.35 mmol, Aldrich), Pd(PPh$_3$)$_4$ (1.47 g, 1.27 mmol, Aldrich) and Na$_2$CO$_3$ (8.08 g, 76.23 mmol, Alfa) were combined under a nitrogen atmosphere in a degassed mixture of *N,N'*-dimethylformamide (DMF, 120 mL) and H$_2$O (40 mL). The mixture was heated at 100 ^{o}C for 72 h and then cooled to room temperature. After removal of the organic solvents, the residue was extracted with CHCl$_3$ (100 mL × 3), and washed with brine (100 mL). The organic phase was dried over anhydrous MgSO$_4$ and filtered. Volatiles were then removed by evaporation under reduced pressure. The residue was purified by silica gel column chromatography to yield the target compound in 56% yield (1.36 g, 3.57 mmol). ^{1}H NMR (CDCl$_3$, 300.0 MHz) δ (ppm): 7.814 (s, 3H), 7.793 (d, *J* = 1.2 Hz, 12 H); ^{13}C NMR (CDCl$_3$, 75.4 MHz) δ (ppm): 144.40, 141.12, 132.74, 127.87, 126.25, 118.50, 111.81; FTIR (neat, cm^{-1}): 2226, 1722, 1602, 1507, 1449, 1394, 1314, 1255, 1209, 1180, 1116, 1017, 974, 904, 823, 737, 700.

4,4',4''-(benzene-1,3,5-triyl-tris(benzene-4,1-diyl))-6,6',6''-tri(1,3,5-triazaine-2,4-diamine) (3-DAT): A mixture of 1,3,5-tri(4-cyanophenyl)benzene (0.90 g, 2.36 mmol), dicyandiamide (0.74 g, 8.80 mmol, Alfa), and powdered KOH (85%, 0.12 g, 1.82 mmol, Aldrich) in 2-methoxyethanol (30 mL, Aldrich) was heated at reflux for 48 hrs. The resulting mixture was cooled and filtered. The solid was extracted thoroughly with hot water. The solid was then rinsed with ethanol and dried in vacuo to give the target compound as a colorless solid in 84% yield (1.26 g, 1.99 mmol). ^{1}H NMR (DMSO-*d$_6$*, 300.0 MHz) δ (ppm): 8.38 (d, *J* = 8.4 Hz, 6H), 8.06 (s, 3H), 8.01 (d, *J* = 8.4 Hz, 6H), 6.81 (s, br, 12H); ^{13}C NMR (DMSO-*d$_6$*, 75.4 MHz) δ (ppm): 169.63, 167.22, 142.18, 140.98, 136.35, 128.17, 126.89, 124.80; FTIR (neat, cm^{-1}): 1632, 1578, 1533, 1449, 1433, 1396, 1255, 1227, 1016, 985, 907, 850, 808, 693, 666.

3. Crystallization of the compound HOF-3

Compound **HOF-3** (350 mg, 0.55 mmol) was dissolved in DMSO (20 mL) under heating. The resulting solution was cooled to room temperature and filtered. The filtrate was divided to 8 small disposable scintillation vials. These vials were then placed inside a large bottle containing THF as a diffusion solvent. The bottle was then closed and kept at room temperature for a month. Colorless block shaped crystals were obtained in 32% yield.

4. The ideal srs net

The ideal **srs** net can be considered as 3_1 (or 3_2) helices of nodes B linked by 3-coordinated (3-c) nodes A. For unit link length the data are: symmetry $R3$, $a = 3$, $c = \sqrt{6}$, A at 0,0,0.; B at 0.25,0,0. This structure is shown in the Figure S4 which might be compared with Figure 1 (c).

5. Fitting of pure component isotherms

Experimental data on pure component isotherms for C_2H_2 and CO_2 were measured at temperatures of 273 K and 296 K. The pure component isotherm data were fitted with the dual-Langmuir isotherm model

$$q = q_{A,sat} \frac{b_A p}{1 + b_A p} + q_{B,sat} \frac{b_B p}{1 + b_B p} \tag{1}$$

The fitted parameter values are presented in Tables S1 and S2 for the data at 273 K, and 296 K, respectively.

As illustration of the goodness of the fits, Figure S7 presents a comparison of component loadings at 296 K in **HOF-3** with the isotherm fits. The fits are good over the entire pressure range.

6. Isosteric heat of adsorption

The binding energies of C_2H_2 and CO_2 in **HOF-3** are reflected in the isosteric heat of adsorption, Q_{st}, defined as

$$Q_{st} = RT^2 \left(\frac{\partial \ln p}{\partial T} \right)_q \tag{2}$$

These values were determined using the pure component isotherm fits. Figure S8 presents data on the loading dependence of Q_{st} in **HOF-3**. Particularly remarkable is the relatively low value of the isosteric heat of adsorption for C_2H_2.

7. Separation of C_2H_2/CO_2 mixtures

The separation of C_2H_2/CO_2 mixtures is important in industry for production of pure C_2H_2, that is required in for a variety of applications in the petrochemical and electronic industries.[1]   The separation is particularly challenging in view of the similarity in the molecular dimensions.[1, 2]

Figure S9 presents IAST calculations of the component loadings for C_2H_2, and CO_2 in a binary equimolar mixture as a function of the total bulk gas phase pressure at 296 K. The IAST calculations indicate the strong separation potential of **HOF-3**.

Three other MOFs: UTSA-30a[3], UTSA-50a[4], and CuBTC[5, 6] are used to compare with **HOF-3** in terms of the adsorption selectivity for separating equimolar C_2H_2/CO_2 mixtures. For CuBTC, the C_2H_2 isotherm fits are from He et al.[5], whereas the CO_2 isotherm fits are those reported by Xiang et al.[6] We note that adsorption selectivity of **HOF-3** is significantly higher than that of other MOFs.

We also performed breakthrough simulations to investigate the separation of C_2H_2/CO_2 mixtures.

8. Column breakthrough test set-up, procedures and measurements

The mixed-gas breakthrough separation experiment was conducted at 296 K using a lab-scale fix-bed reactor as illustrated in the scheme below.
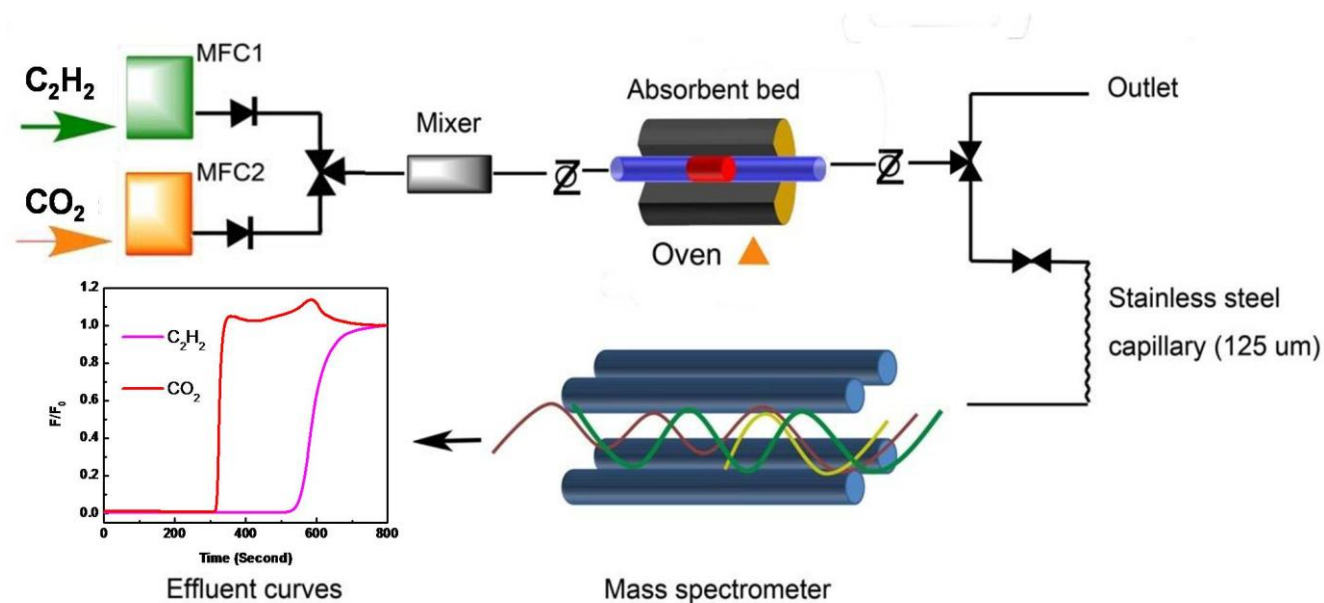
In a typical experiment, 970 mg of **HOF-3** powder was packed into a quartz column (5.8 mm I.D. × 150 mm) with silica wool filling the void space. The sorbent was activated *in situ* in the column with a vacuum pump at 296 K for 24 h. A helium flow (5 cm^3 min^{-1}) was used introduced after the activation process to purge the adsorbent. The flow of He was then turned off while a gas mixture of C_2H_2/CO_2 (50 : 50, v/v) at 5 cm^3 min^{-1} was allowed to flow into the column. The effluent from the column was monitored using a mass spectrometer (MS). The absolute adsorbed amount of gas i (q_i) is calculated from the breakthrough curve by the equation:

$$q_i = \frac{F_i \times t_0 - V_{dead} - \int_0^{t_0} F_e \Delta t}{m} \tag{3}$$

where F_i is the influent flow rate of the specific gas (cm^3 min^{-1}); t_0 is the adsorption time (min); V_{dead} is the dead volume of the system (cm^3); F_e is the effluent flow rate of the specific gas (cm^3 min^{-1}); and m is the mass of the sorbent (g).

The separation factor (α) of the breakthrough experiment is determined as

$$\alpha = \frac{q_1}{y_1} \times \frac{q_2}{y_2} \tag{4}$$

where y_i is the molar fraction of gas i in the gas mixture.

In this case, the adsorbed amounts of C_2H_2 and CO_2 are calculated to be 1.14 mmol/g and 0.56 mmol/g, respectively. Accordingly, the separation factor is α = 2.04.

9. Simulation methodology for transient breakthrough in fixed bed adsorbers

Fixed bed, packed with crystals of nanoporousmaterials, are commonly used for separation of mixtures (see schematic in Figure S10); such adsorbers are commonly operated in a transient mode, and the compositions of the gas phase, and within the crystals, vary with position and time. For a given separation task, transient breakthroughs provide more a realistic evaluation of the efficacy of a material, as they reflect the combined influence of adsorption selectivity, and adsorption capacity.[2, 3]

Assuming plug flow of an *n*-component gas mixture through a fixed bed maintained under isothermal conditions, the partial pressures in the gas phase at any position and instant of time are obtained by solving the following set of partial differential equations for each of the species i in the gas mixture.[4]

$$\frac{1}{RT}\frac{\partial p_i(t,z)}{\partial t} = -\frac{1}{RT}\frac{\partial(v(t,z)p_i(t,z))}{\partial z} - \frac{(1-\varepsilon)}{\varepsilon}\rho\frac{\partial \bar{q}_i(t,z)}{\partial t}; \quad i=1,2,...n \tag{5}$$

In equation (5), t is the time, z is the distance along the adsorber, ρ is the framework density, ε is the bed voidage, v is the interstitial gas velocity, and $\bar{q}_i(t,z)$ is the *spatiallyaveraged* molar loading within the crystallites of radius r_c, monitored at position z, and at time t.

At any time t, during the transient approach to thermodynamic equilibrium, the spatially averaged molar loading within the crystallite r_c is obtained by integration of the radial loading profile

$$\bar{q}_i(t) = \frac{3}{r_c^3}\int_0^{r_c} q_i(r,t)r^2 dr \tag{6}$$

If the value of the intra-crystalline diffusivity is large enough to ensure that intra-crystalline gradients are absent and the entire crystallite particle can be considered to be in thermodynamic equilibrium with the surrounding bulk gas phase at that time t, and position z of the adsorber

$$\overline{q}_i(t,z) = q_i(t,z) \tag{7}$$

The *interstitial* gas velocity is related to the *superficial* gas velocity by

$$v = \frac{u}{\varepsilon} \tag{8}$$

In industrial practice, the most common operation is with to use a step-wise input of mixtures to be separation into an adsorber bed that is initially free of adsorbates, i.e. we have the initial condition

$$t = 0; \quad q_i(0,z) = 0 \tag{9}$$

At time, $t = 0$, the inlet to the adsorber, $z = 0$, is subjected to a step input of the *n*-component gas mixture and this step input is maintained till the end of the adsorption cycle when steady-state conditions are reached.

$$t \geq 0; \quad p_i(0,t) = p_{i0}; \quad u(0,t) = u_0 \tag{10}$$

where u_0 is the superficial gas velocity at the inlet to the adsorber.

Besides, the breakthrough simulations with a step-input (10), we also carried out simulations for a pulse chromatographic separation device with injection of a short duration pulse of the mixture to be separated. For simulation of pulse chromatographic separations, we use the corresponding set of inlet conditions

$$0 \leq t \leq t_0; \quad p_i(0,t) = p_{i0}; \quad u(0,t) = u_0 \tag{11}$$

where the time for duration of the pulse is t_0.

It is to be noted that the actual values of these parameters have no real bearing on the conclusions drawn on the separation performance and for this reason the simulation results for transient breakthrough are presented in our investigation in terms of a *dimensionless* time, τ, defined by dividing the actual time, t, by the characteristic time, $\frac{L\varepsilon}{u_0}$.

10. Transient breakthrough of C$_2$H$_2$/CO$_2$ mixtures

In view of the extremely high selectivity for adsorption of C_2H_2, it is possible to recover pure CO_2 during the adsorption phase in a fixed bed adsorber; An important advantage of **HOF-3** over the three MOFs UTSA-30a[3], UTSA-50a[4], and CuBTC[5] is the significantly lower binding energy for C_2H_2;. The lower binding energy implies significantly lower regeneration energy requirements.

11.   Notation

b	Langmuir constant, $Pa^{-\nu_i}$
L	length of packed bed adsorber, m
n	number of species in the mixture, dimensionless
p_i	partial pressure of species i in mixture, Pa
p_t	total system pressure, Pa
q_i	component molar loading of species i, mol kg^{-1}
$q_{i,sat}$	molar loading of species i at saturation, mol kg^{-1}
q_t	total molar loading in mixture, mol kg^{-1}
q_{sat}	saturation loading, mol kg^{-1}
$\overline{q}_i(t)$	*spatiallyaveraged* component molar loading of species i, mol kg^{-1}
r	radial direction coordinate, m
r_c	radius of crystallite, m
R	gas constant, 8.314 J mol^{-1} K^{-1}
t	time, s
T	absolute temperature, K
u	superficial gas velocity in packed bed, m s^{-1}
v	interstitial gas velocity in packed bed, m s^{-1}
x_i	mole fraction of species i in adsorbed phase, dimensionless
z	distance along the adsorber, and along membrane layer, m

Greek letters

ε	voidage of packed bed, dimensionless
ρ	framework density, kg m^{-3}
τ	time, dimensionless

Subscripts

i	referring to component i
t	referring to total mixture

12.   Details of DFT-D calculations and GCMC simulations

First-principles calculations based on density-functional theory were performed using the PWSCF package.[10] A semiempirical addition of dispersive forces to conventional DFT[11] was included in the calculation to account for van der Waals interactions. We used Vanderbilt-type ultrasoft pseudopotentials and the generalized gradient approximation (GGA) with the Perdew-Burke-Ernzerhof (PBE) exchange correlation. A cutoff energy of 544 eV and a 2x2x2 k sampling were sufficient for the total energy to converge within 0.5 meV/atom. We first optimized the bare **HOF-3** structure. The optimized structure is fairly close to the experimental structure determined from XRD, confirming the framework connection being H-bonded. C_2H_2 or CO_2 molecules were then introduced to the optimized

HOF structure (guided by the GCMC result), followed by a full structural relaxation. To obtain the gas binding energies, a free gas molecule placed in a supercell with the same cell dimensions was also relaxed as a reference. The static binding energy was then calculated using: $E_B = [E(MOF) + nE(gas) − E(MOF + ngas)]/n$. Interestingly, we found that the **HOF-3** framework is quite flexible, and introduction of guest gas molecules leads to notable relaxation of the framework itself (e.g., changes of the angles between the phenyl rings and the DAT groups). Nevertheless, the framework is overall robust and all building units are still connected in the same fashion through H-bonding, as in bare **HOF-3** structure.

Grand Canonical Monte Carlo (GCMC) simulations[12] were performed for C_2H_2/CO_2 adsorption in **HOF-3**, with the gas molecules and the HOF frameworks both treated as rigid bodies. A $2\times2\times2$ supercell was used as the simulation box to ensure the simulation accuracy. 2×10^7 steps were used for equilibration and additional 2×10^7 steps were used to calculate the ensemble average of gas adsorption sites and thermodynamic properties. We used the standard universal force field (UFF)[13] to describe the gas-framework interaction and the gas-gas interaction. Atomic partial charges derived from first-principles calculation were included in the simulation to account for electrostatic interactions. The cut-off radius used for the Lennard-Jones interactions is 12.8 Å. The long-range electrostatic interactions were treated using the Ewald summation technique with tin-foil boundary condition. Simulations were performed at various temperatures and pressures. The probability distributions of adsorbed C_2H_2 and CO_2 were generated from the simulation after the equilibrium stage, and representative results are shown in Figure S12 as examples.

Disclaimer: Certain commercial equipment, instruments, or materials are identified in this paper to foster understanding. Such identification does not imply recommendation or endorsement by the National Institute of Standards and Technology, nor does it imply that the materials or equipment identified are necessarily the best available for the purpose.

Table S1. Dual-Langmuir parameter fits for **HOF-3** at 273 K.

	Site A		Site B	
	$q_{A,sat}$ mol kg^{-1}	b_A Pa^{-1}	$q_{B,sat}$ mol kg^{-1}	b_B Pa^{-1}
C_2H_2	1.7	4.17×10^{-4}	1.4	7.12×10^{-6}
CO_2	1	9.31×10^{-5}	1.9	3.92×10^{-6}

Table S2. Dual-Langmuir parameter fits for **HOF-3** at 296 K.

	Site A		Site B	
	$q_{A,sat}$ mol kg^{-1}	b_A Pa^{-1}	$q_{B,sat}$ mol kg^{-1}	b_B Pa^{-1}
C_2H_2	1.5	2.11×10^{-4}	1.3	9.91×10^{-6}
CO_2	1.4	1.7×10^{-5}	0.1	1.01×10^{-6}
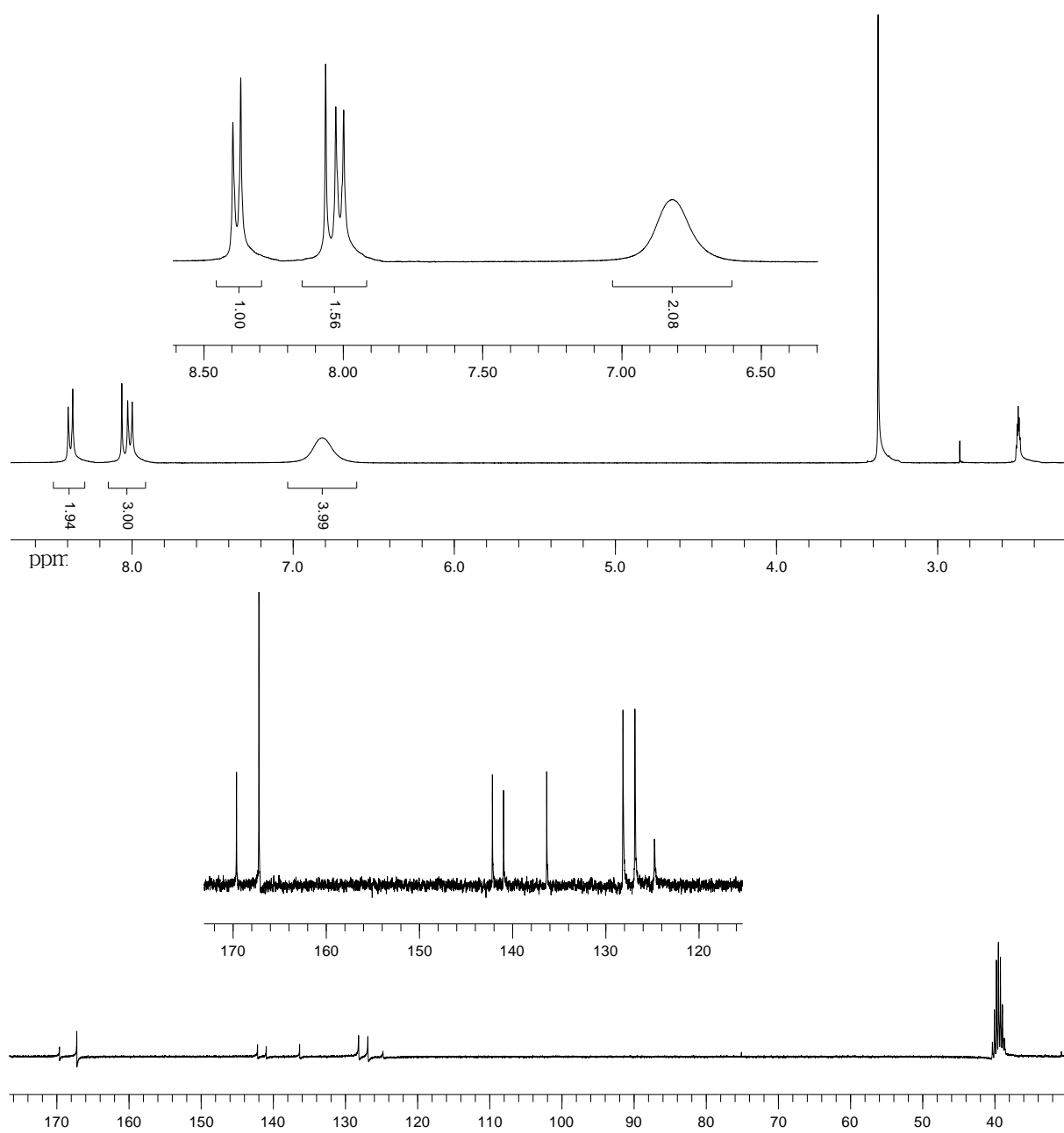
Figure S1 ^{1}H NMR (DMSO-d$_6$, 300.0 MHz) and ^{13}C NMR (DMSO-d$_6$, 75.4 MHz) spectra of the organic linker.
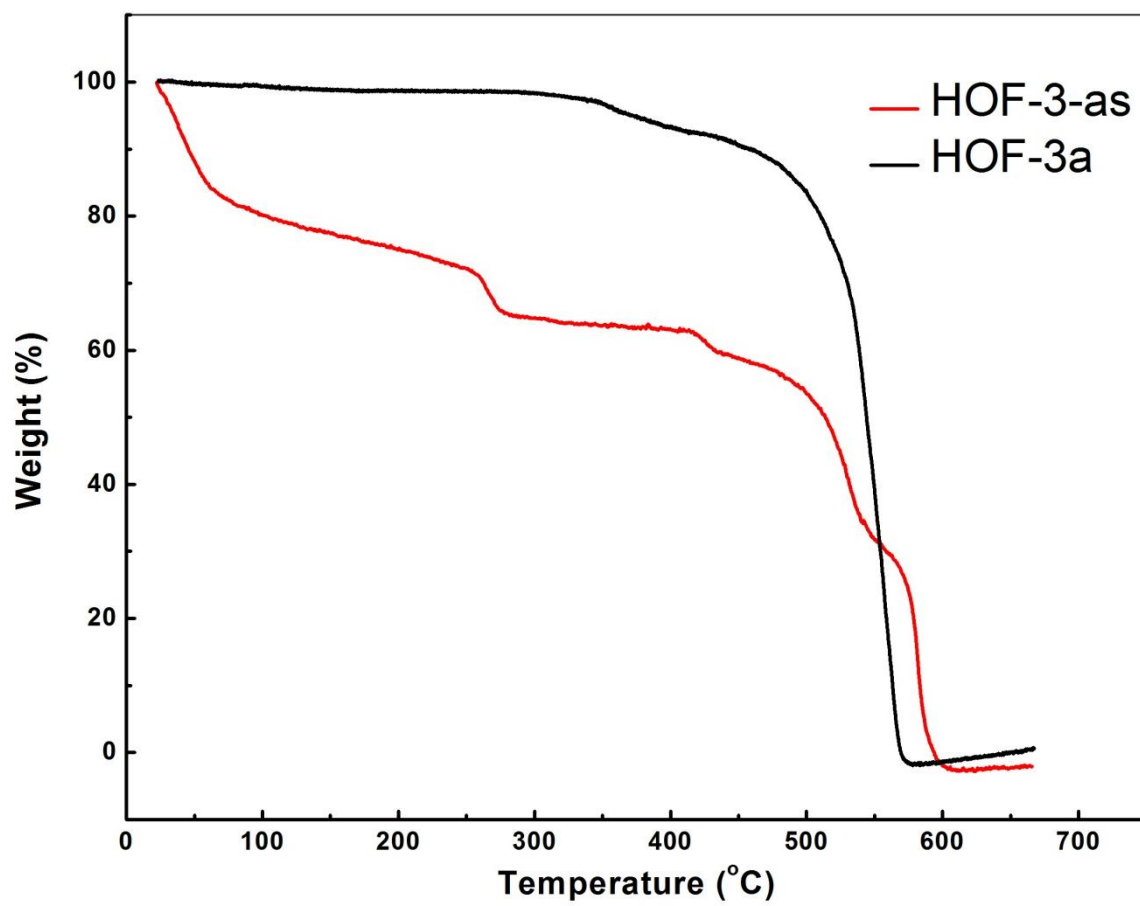
Figure S2 TGA curves of as-synthesized **HOF-3** (red) and **HOF-3a** (black).
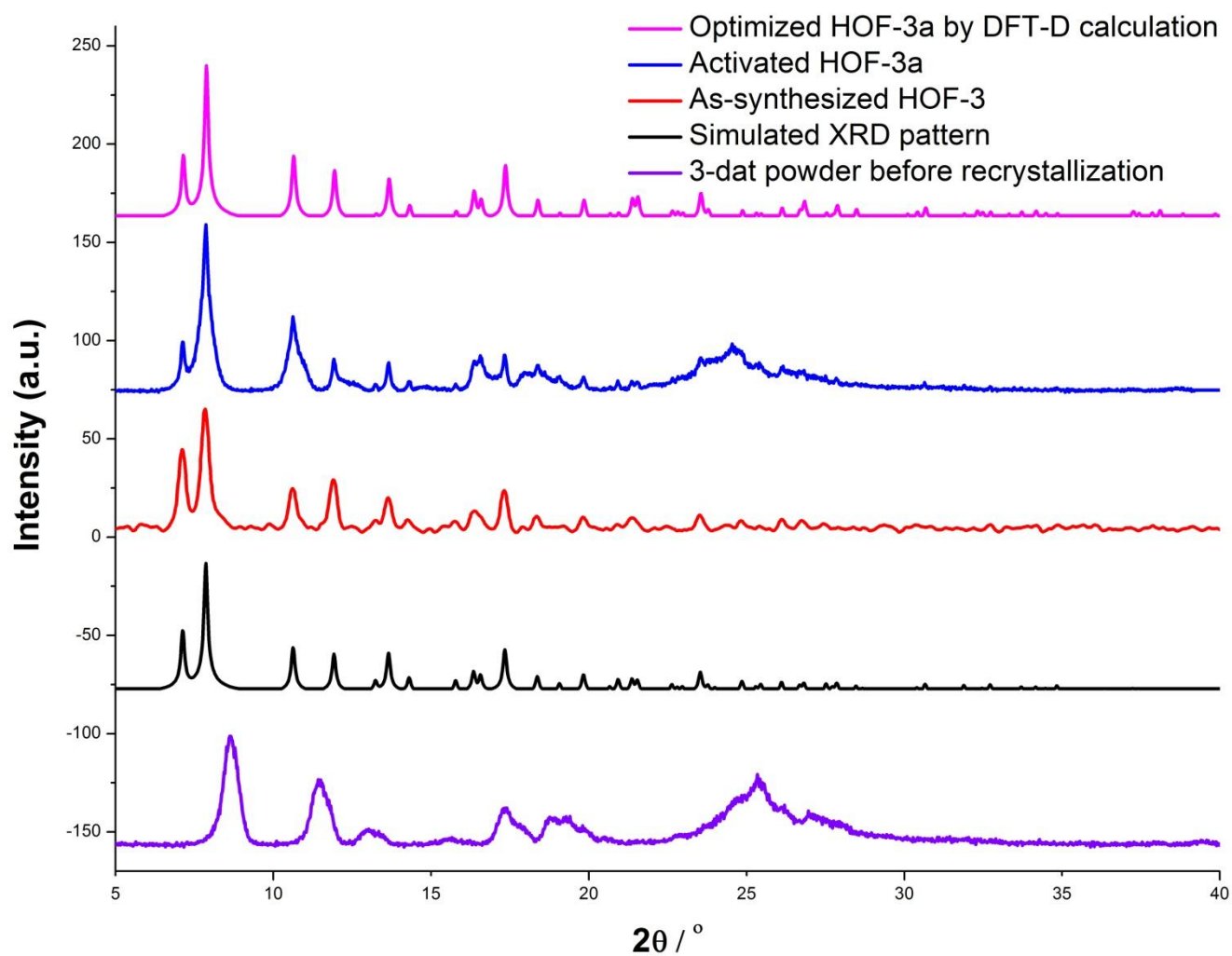
Figure S3 Powder X-ray diffraction patterns of the as-synthesized 3-DAT, as-synthesized **HOF-3** and activated **HOF-3a**, and comparision with those simulated ones from structurally characterized **HOF-3** and simulated **HOF-3a**.
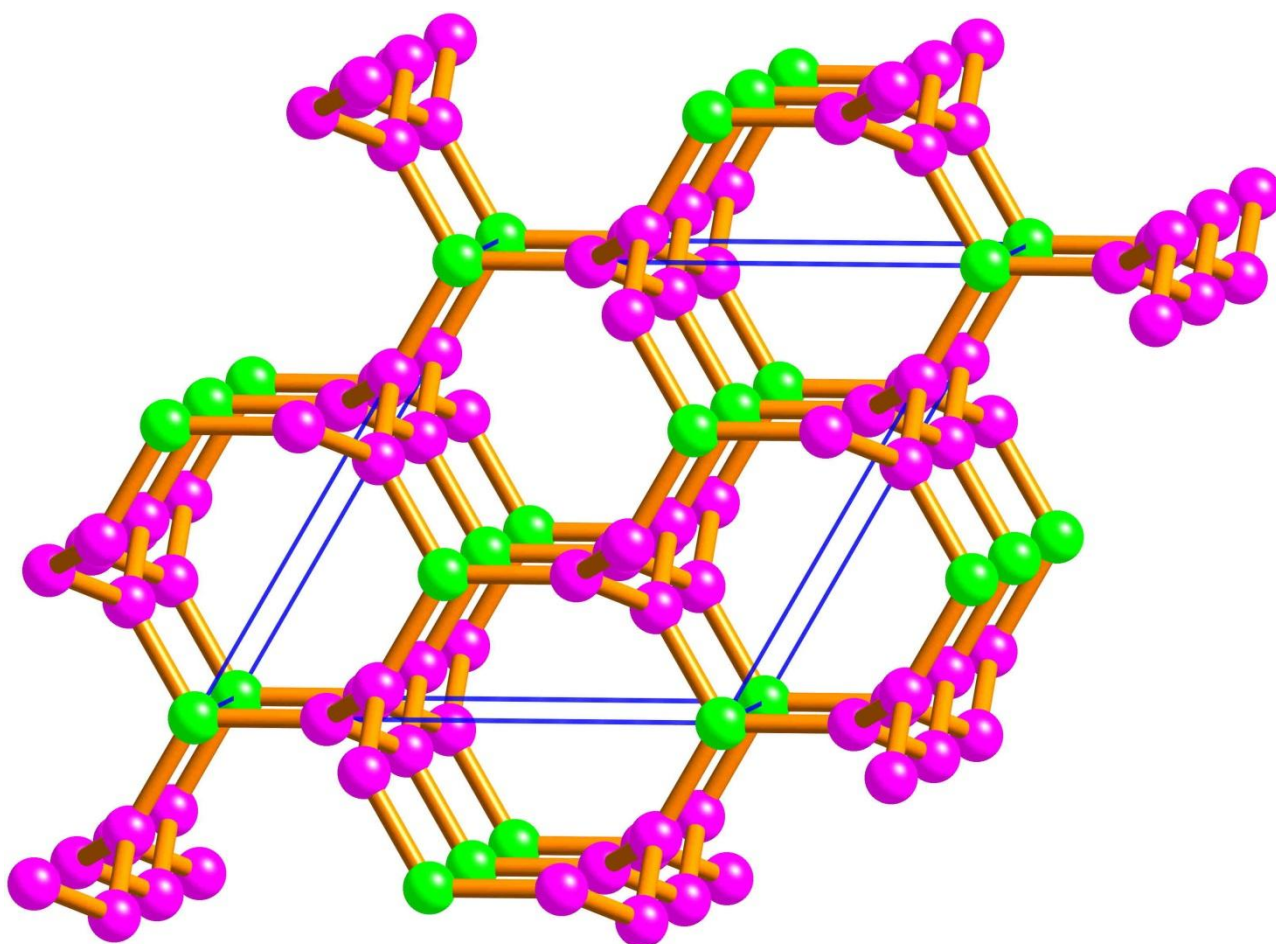
Figure S4 The ideal **srs** net. Green balls stand for node A and magenta balls stand for node B in 3-fold helical rods.
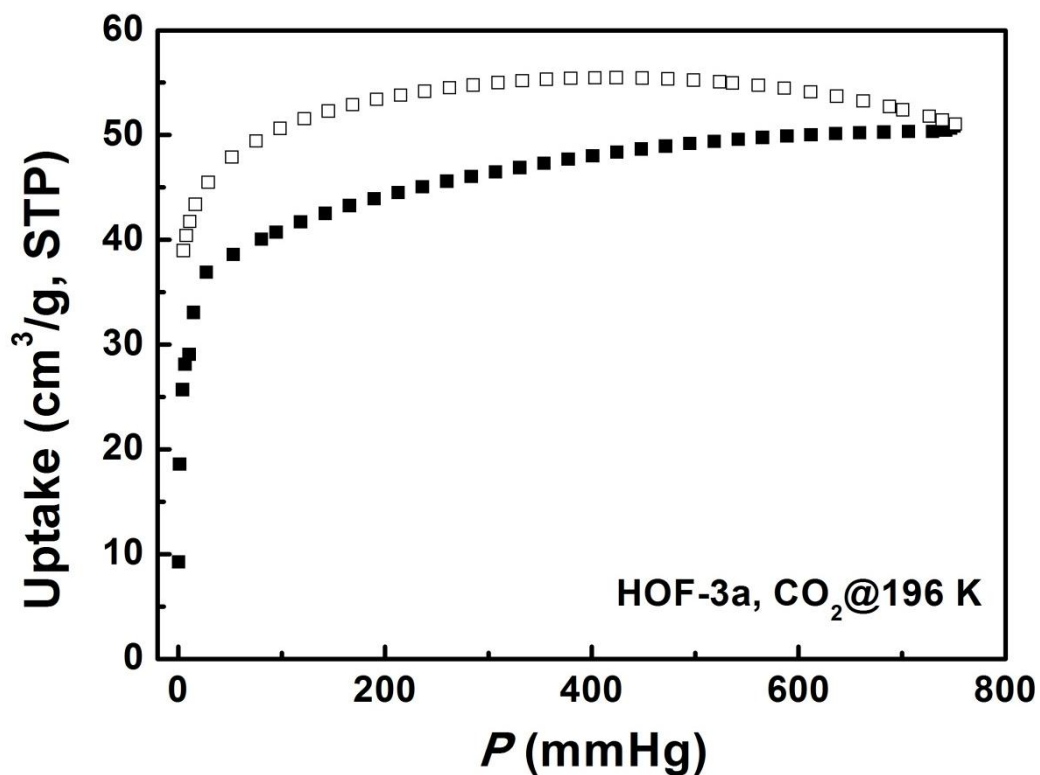
Figure S5 CO_2 sorption isotherm of **HOF-3a** at 196 K.
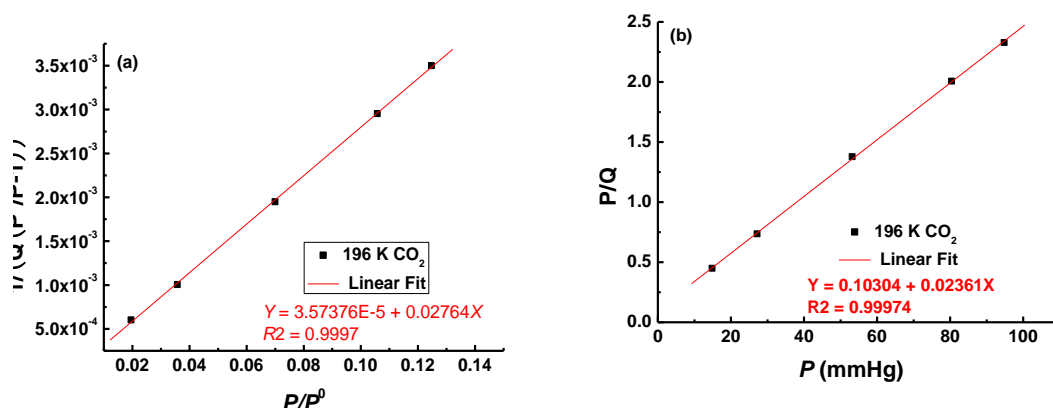
$S_{BET} = (1/(0.02764 + 0.0000357376))/22414 \times 6.023 \times 10^{23} \times 0.170 \times 10^{-18} = 165.0 \text{ m}^2/\text{g}$

$S_{Langmuir} = (1/0.02361)/22414 \times 6.023 \times 10^{23} \times 0.170 \times 10^{-18} = 193.5 \text{ m}^2/\text{g}$
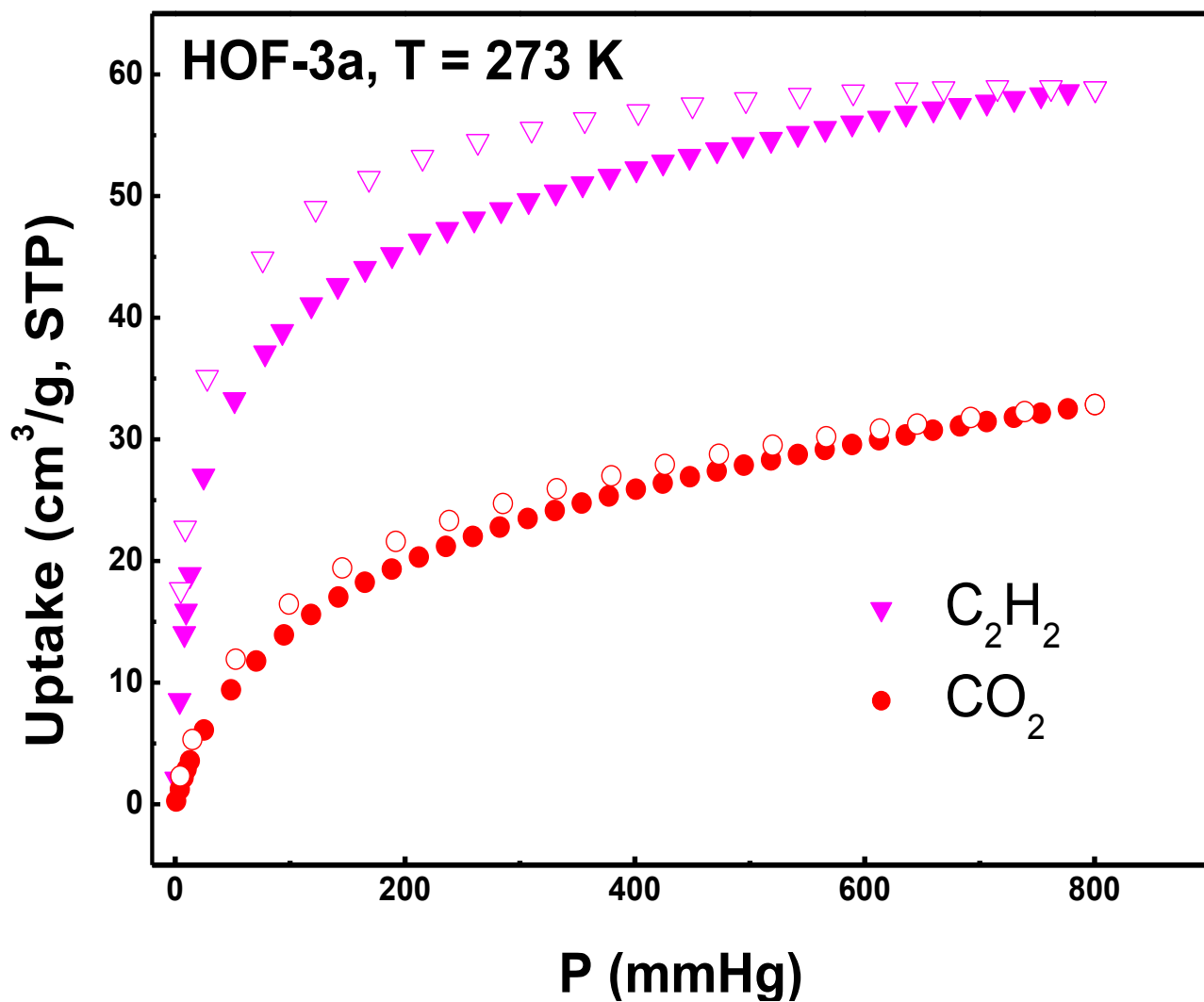
Figure S6 Gas sorption isotherms for C_2H_2 and CO_2 in **HOF-3a** at 273 K.
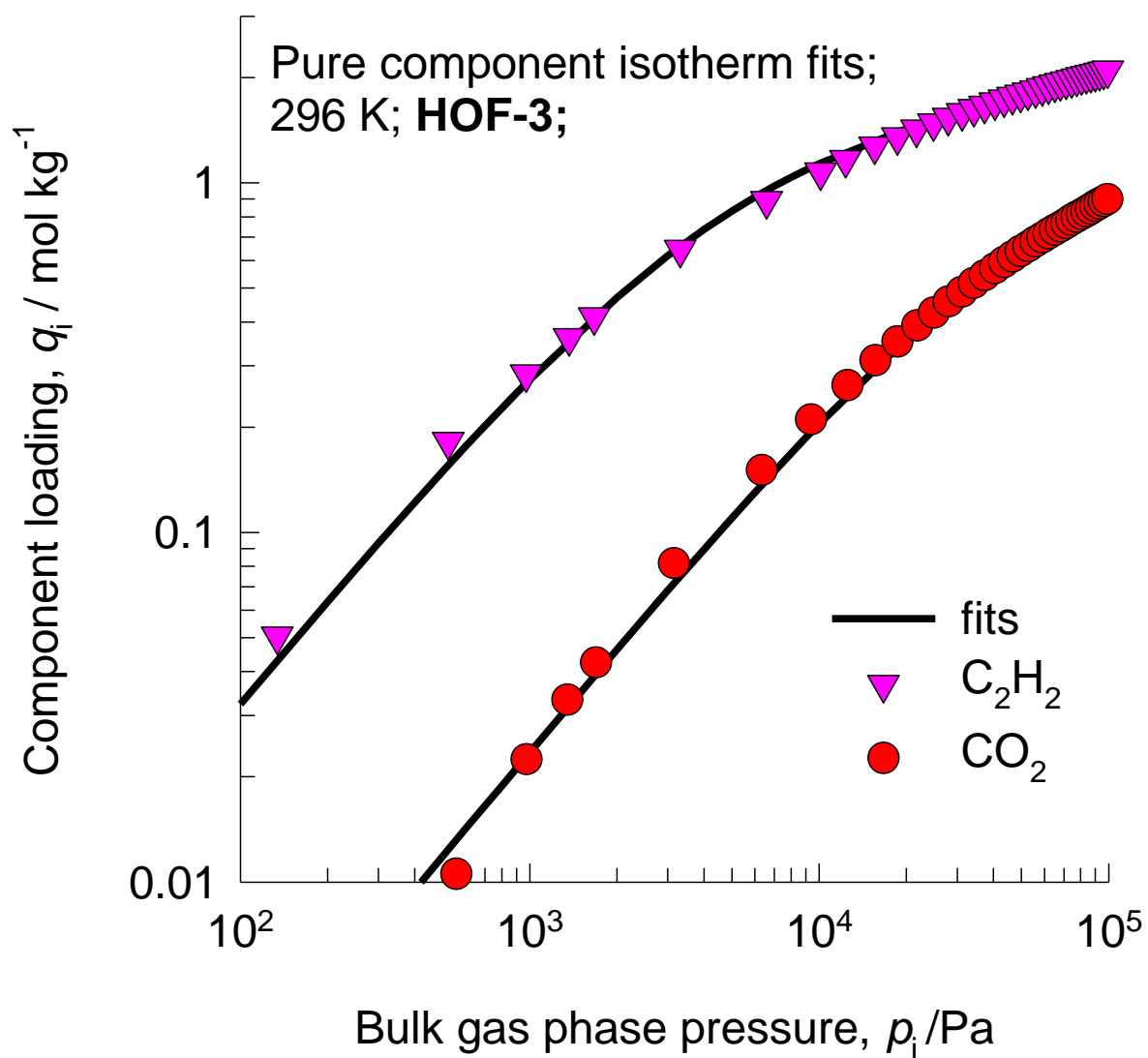
Figure S7 Comparison of absolute component loadings for C_2H_2 and CO_2 at 296 K in **HOF-3** with the dual-Langmuir isotherm fits.
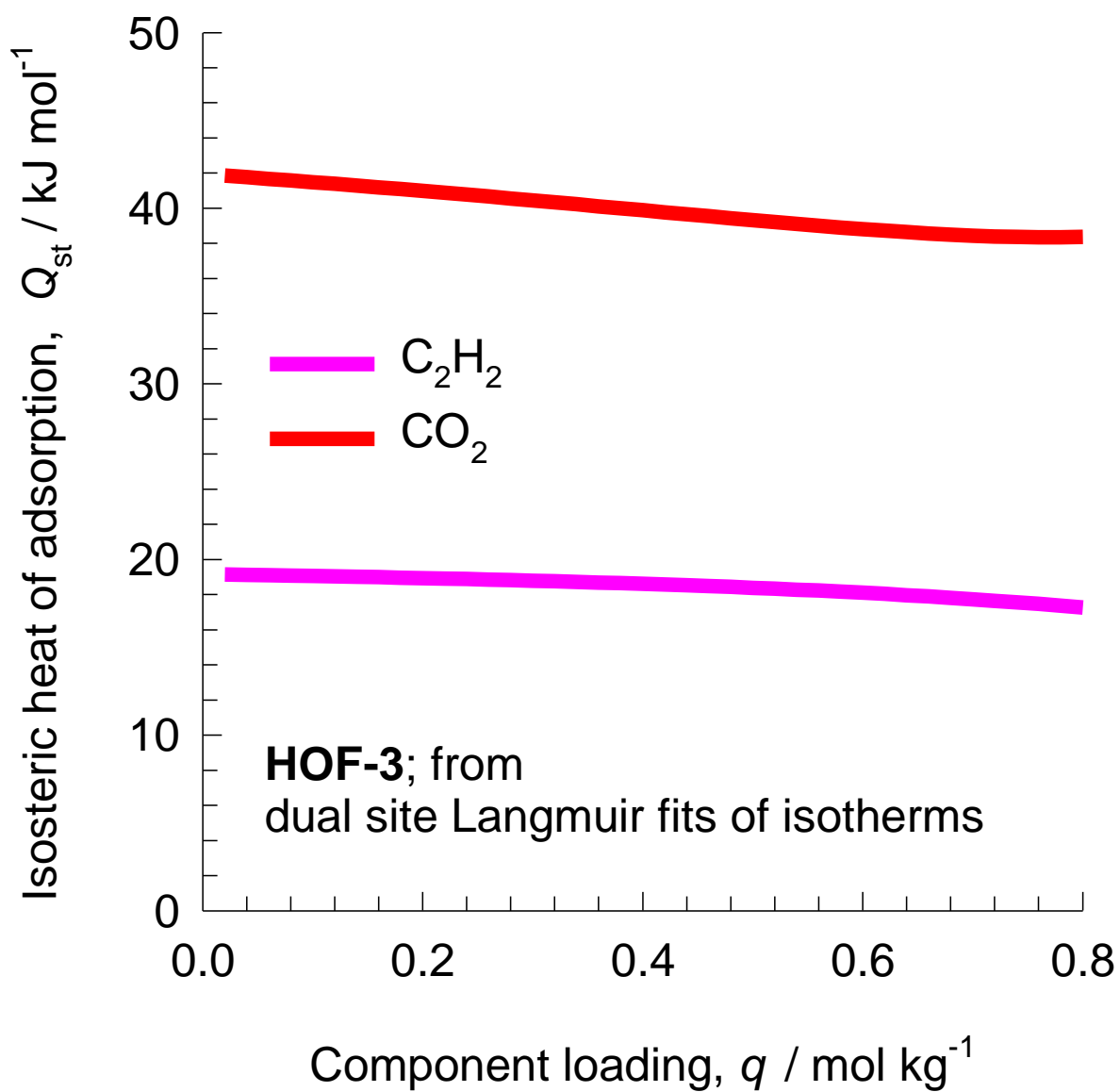
Figure S8 The isosteric heat of adsorption for C_2H_2 and CO_2 in **HOF-3.** The determination of the Q_{st} is based on the Clausius-Clapeyron equation.
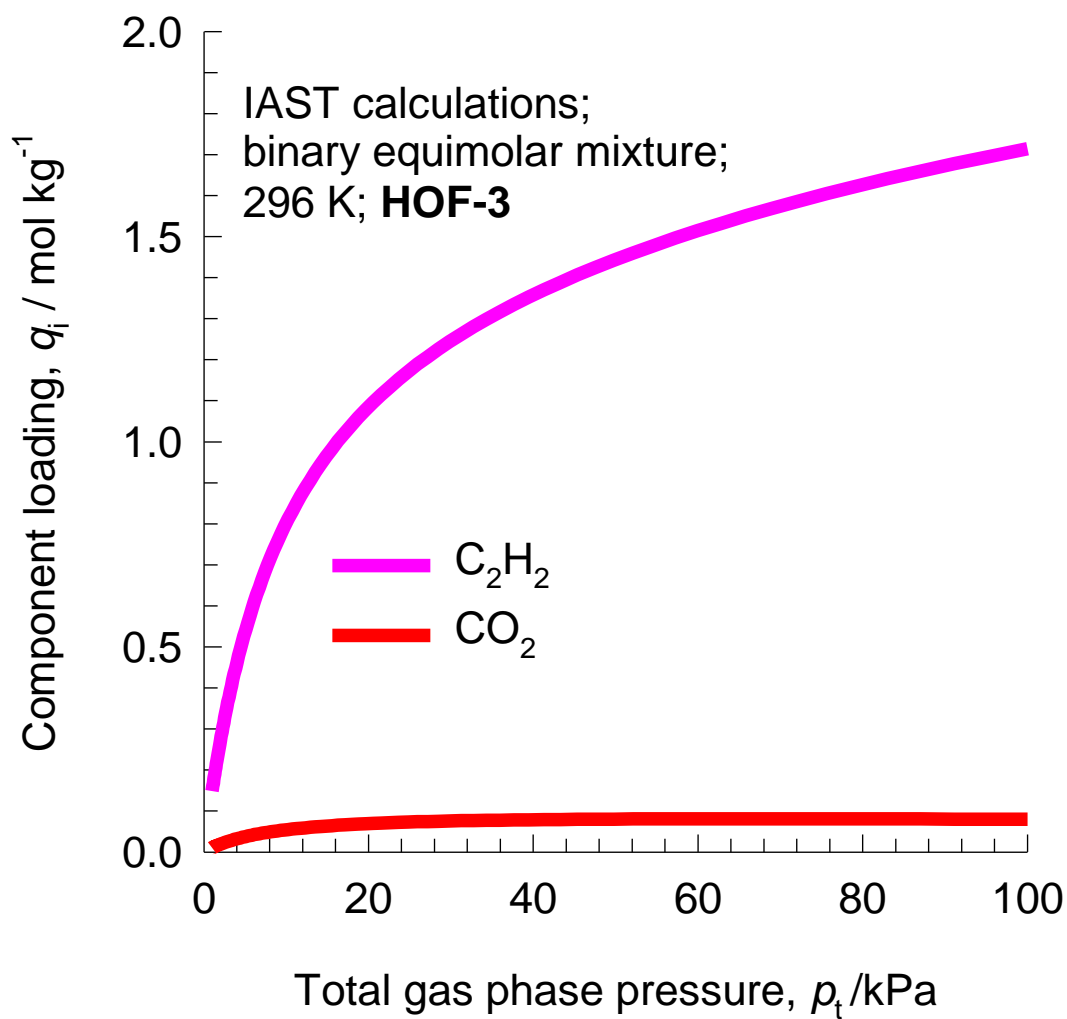
Figure S9 IAST calculations of the component loadings for C_2H_2, and CO_2 in a binary equimolar mixture as a function of the total bulk gas phase pressure at 296 K.
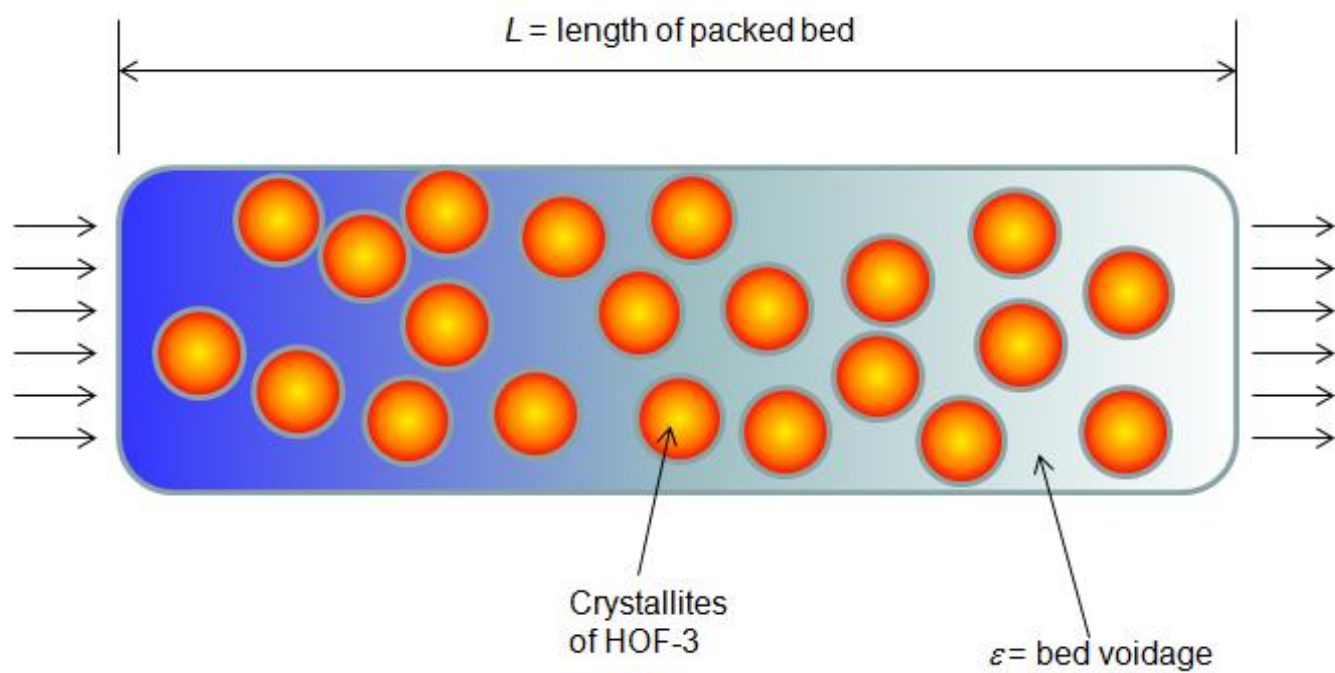
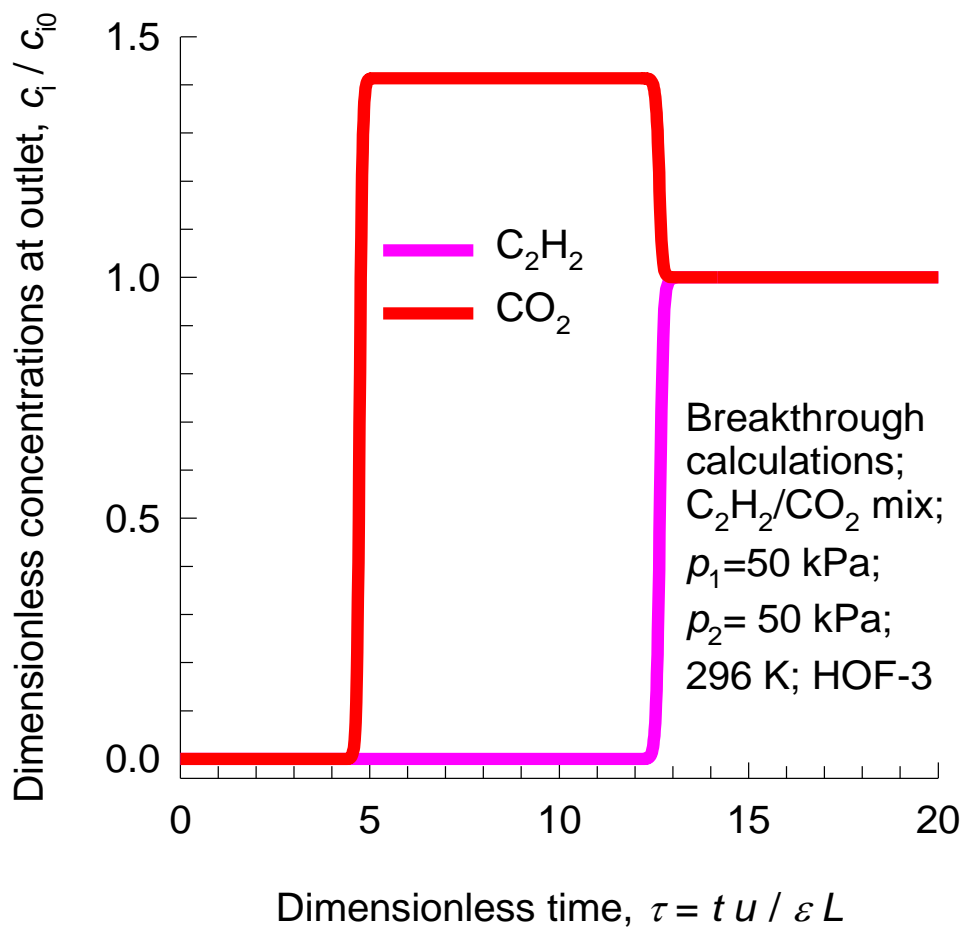**Figure S10** Schematic of a fixed bed adsorber packed with **HOF-3a**.

Figure S11 Transient breakthrough of equimolar C_2H_2/CO_2 mixture in an adsorber bed packed with **HOF-3a**. The total bulk gas phase is at 296 K and 100 kPa. For the breakthrough simulations, the following parameter values were used, $L = 0.12$ m; $\varepsilon = 0.75$; $u_0 = 0.00225$ m/s.
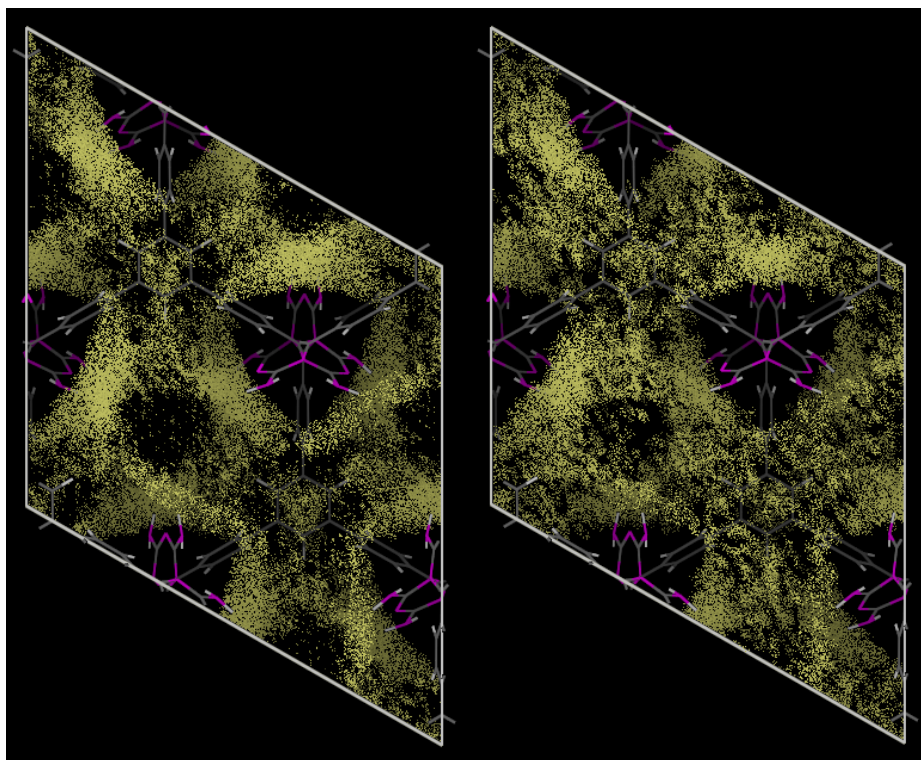
Figure S12 Probability distribution of the C_2H_2 (left) and CO_2 (right) center of mass in **HOF-3** unit cell, obtained from GCMC simulation at 296 K, and 1 bar. The yellow regions represent the places where gas molecules are populated in the HOF structure.
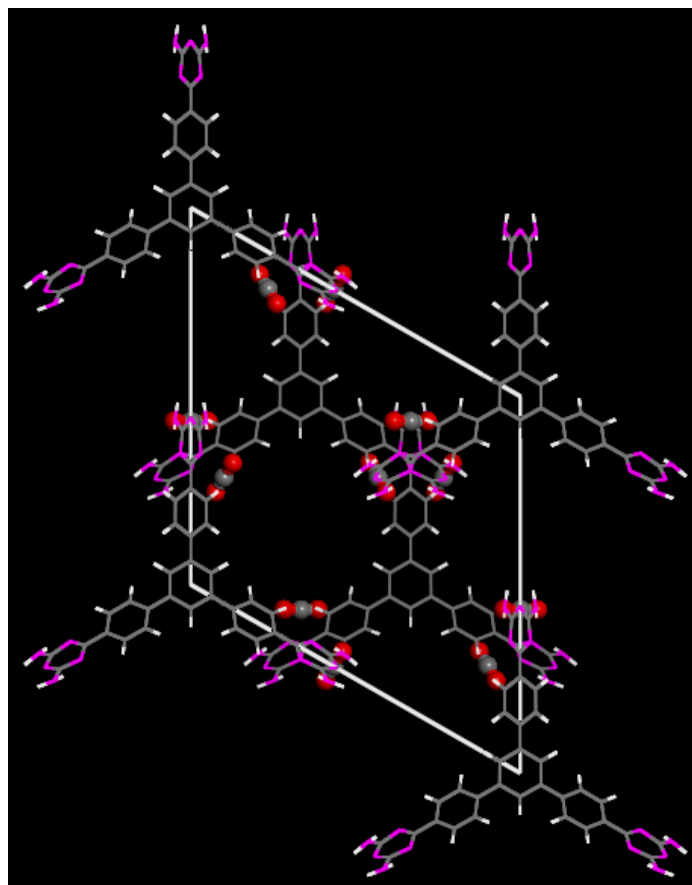
Figure S13 DFT-D optimized structure of the **HOF-3** crystal with CO_2 molecules adsorbed on the "pocket" sites.

13. References

1.   R. Matsuda, R. Kitaura, S. Kitagawa, Y. Kubota, R. V. Belosludov, T. C. Kobayashi, H. Sakamoto, T. Chiba, M. Takata, Y. Kawazoe, Y. Mita, *Nature* **2005,***436*, 238.

2.   M. Fischer, F. Hoffmann, M. Fröba, *ChemPhysChem* **2010,***11*, 2220.

3.   Y. He, S. Xiang, Z. Zhang, S. Xiong, F. R. Fronczek, R. Krishna, M. O'Keeffe, B. Chen, *Chem. Commun.* **2012,***48*, 10856.

4.   H. Xu, Y. He, Z. Zhang, S. Xiang, S. Xiong, J. Cai, Y. Cui, Y. Yang, G. Qian, B. Chen, *J. Mater. Chem. A* **2013,***1*, 77.

5.   Y. He, R. Krishna, B. Chen, *Energy Environ. Sci.* **2012,***5*, 9107.

6.   S. Xiang, Y. He, Z. Zhang, H. Wu, W. Zhou, R. Krishna, B. Chen, *Nat. Commun.* **2012,***3*, 954.

7.   R. Krishna, J. R. Long, *J. Phys. Chem. C* **2011,***115*, 12941.

8.   R. Krishna, *Microporous Mesoporous Mater.* **2014,***185*, 30.

9.   R. Krishna, R. Baur, *Sep. Purif. Technol.* **2003,***33*, 213.

10.   P. Giannozzi, S. Baroni, N. Bonini, M. Calandra, R. Car, C. Cavazzoni, D. Ceresoli, G. L. Chiarotti, M. Cococcioni, I. Dabo, A. Dal Corso, S. Fabris, G. Fratesi, S. de Gironcoli, R. Gebauer, U. Gerstmann, C. Gougoussis, A. Kokalj, M. Lazzeri, L. Martin-Samos, N. Marzari, F. Mauri, R. Mazzarello, S. Paolini, A. Pasquarello, L. Paulatto, C. Sbraccia, S. Scandolo, G. Sclauzero, A. P. Seitsonen, A. Smogunov, P. Umari, R. M. Wentzcovitch, *J. Phys.: Condens. Matter***2009**, *21*, 395502.

11. V. Barone, M. Casarin, D. Forrer, M. Pavone, M. Sambi, A. J. Vittadini, *Comput. Chem.***2009**, *30*, 934.

12. Frenkel and B. Smit, Understanding Molecular Simulation: From Algorithms to Applications. San Diego: *Academic Press*, **2002**.

13. A. K. Rappi, C. J. Casewit, K. S. Colwell, W. A. Goddard III, W. M. Skid, W. M. *J. Am. Chem. Soc.* **1992**, *114*, 10024.